Hard-disk equation of state: First-order liquid-hexatic transition in two dimensions with three simulation methods

Joshua A. Anderson,[1] Michael Engel,[1] Sharon C. Glotzer,[1,*]
Masaharu Isobe,[2,3] Etienne P. Bernard,[4] and Werner Krauth[5,†]

[1]*Department of Chemical Engineering, University of Michigan, Ann Arbor, Michigan 48109, USA*
[2]*Graduate School of Engineering, Nagoya Institute of Technology, Nagoya, 466-8555, Japan*
[3]*Department of Chemistry, University of California, Berkeley, California 94720, USA*
[4]*Department of Physics, Massachusetts Institute of Technology, Cambridge, Massachusetts 02139, USA*
[5]*Laboratoire de Physique Statistique, École Normale Supérieure, UPMC, CNRS, 24 Rue Lhomond, 75231 Paris Cedex 05, France*

(Dated: November 8, 2012)

We report large-scale computer simulations of the hard-disk system at high densities in the region of the melting transition. Our simulations reproduce the equation of state, previously obtained using the event-chain Monte Carlo algorithm, with a massively parallel implementation of the local Monte Carlo method and with event-driven molecular dynamics. We analyze the relative performance of these simulation methods to sample configuration space and approach equilibrium. Phase coexistence is visualized for individual configurations via the local orientations, and positional correlation functions are computed. Our results confirm the first-order nature of the liquid-hexatic phase transition in hard disks.

PACS numbers: 05.70.Fh, 64.70.dj, 61.20.Ja, 33.15.Vb

I. INTRODUCTION

The phase behavior of hard disks is one of the oldest and most studied problems in statistical mechanics. It inspired the use of Markov-chain Monte Carlo [1] as well as molecular dynamics [2]. Important progress in understanding hard-disk melting [3–5] was made recently. Using the event-chain Monte Carlo algorithm (ECMC) [6], a first-order liquid-hexatic transition was identified [7]. This transition from the low-density phase to an intermediate phase precedes a continuous hexatic-solid transition, and thus the liquid transforms to a solid through an intermediate hexatic phase.

Controversy concerning the nature of hard-disk melting has persisted for decades. Indeed, the recently discovered first-order liquid-hexatic melting transition differs from the standard KTHNY scenario [8–13], which predicts continuous transitions both from the liquid to the hexatic and from the hexatic to the solid. It is also at variance with the first-order liquid-solid transition scenario, which exhibits no intermediate hexatic phase and has been much discussed [3, 13–18]. Near the critical density, the system is correlated across roughly a hundred disk radii, and the hard-disk liquid-hexatic transition is thus weakly first-order [7], with only a small discontinuity in density at the transition.

For several decades, the algorithms used for this problem [12, 13, 18–20] were unable to equilibrate systems sufficiently larger than the spatial correlation length to reliably investigate the existence and the nature of the hexatic phase. This was one origin for the controversy surrounding this problem. Another reason was that the manifestation of a first-order transition in the NVT ensemble, and in particular the fundamental difference between a van der Waals loop and a Mayer-Wood loop indicating equilibrium phase coexistence, was not universally accepted in the hard-disk community, although it had been clearly discussed in the literature [21–23].

Here, we complement and compare the recent event-chain results with a massively parallel implementation of the local Monte Carlo algorithm (MPMC) [24], and with event-driven molecular dynamics (EDMD) [25]. These methods provide us with by far the largest independent data sets ever acquired for the hard-disk melting transition, allowing us to reproduce to very high precision the equation of state of Ref. [7], obtain snapshots illustrating phase separation, and compute positional correlation functions.

II. SIMULATION METHODS

A. System definition

We consider a system of N hard disks of radius σ in a square box of size $L \times L$. The phase diagram of the system depends only on the density (packing fraction) $\eta = N\pi\sigma^2/L^2$, as the pressure is proportional to the temperature T. The dimensionless pressure is given by

$$P^* = \frac{(2\sigma)^2}{m\langle v_x^2\rangle} P = \beta P (2\sigma)^2 \tag{1}$$

with the inverse temperature β, mass m and the velocity along one axis v_x. All simulations are conducted in

*Electronic address: sglotzer@umich.edu
†Electronic address: werner.krauth@ens.fr

the NVT ensemble and, although our algorithms differ in the way they evolve the system, they all sample the same equilibrium probability distribution in configuration space. At finite N, the equilibrium phase coexistence that we will observe is specific to this ensemble and absent, for example, in the NPT ensemble. As for any model with short-range interactions, the thermodynamic limit is independent of the ensemble.

B. Algorithms and implementations

Local Monte Carlo (LMC) has been a popular simulation method for hard disks [1, 13, 18, 20]. At each time step, one random disk is selected and a trial move is applied to it. The move is accepted unless it results in an overlap with another disk. LMC is both relatively inefficient in sampling configuration space and inherently serial, limiting the size for which the system can be brought to equilibrium at high densities $\eta \sim 0.7$ to about $N \sim 10^5$ particles (see [26] for a basic discussion). Our alternative approaches utilize modern computer resources more efficiently and equilibrate the system faster. They also provide independent checks of the equilibrium phase behavior. LMC is used for comparison and as a reference to previous work.

Massively parallel Monte Carlo (MPMC) [24] is a parallel extension of LMC. It again applies a local trial move, but maximizes the number of simultaneous updates. MPMC extends the stripe decomposition method [27] to a massive number of threads using a four-color checkerboard scheme [28]. By placing disks into cells of width $w \gtrsim 2\sigma$, concurrent threads execute over one out of four subsets of cells in parallel. Within each cell, particles are chosen for trial moves in a shuffled order. The number of trial moves is fixed independent of cell occupancy. Trial moves that would displace disks across cell boundaries are rejected. The order of the four checkerboard sub-sweeps is also sampled as a random permutation. In this manner, an entire sweep over N particles satisfies detailed balance. The reverse sweep corresponds to an inverse shuffling and cell sequences with opposite trial moves and occurs with equal probability. To ensure ergodicity, the cell system is randomly shifted after each sweep. We implement MPMC on a graphics processing unit (GPU) using CUDA. Details are found in Ref. [24]. The MPMC simulations execute simultaneously on all 1536 cores of a NVIDIA GeForce GTX 680.

In event-driven molecular dynamics (EDMD), individual simulation events correspond to collisions between pairs of disks [2]. The simulation is advanced sequentially from one collision event to the next. Between collisions, disks move at constant velocity (see [26] for a basic discussion). The computation of future collisions and the update of the event schedule are performed efficiently using a binary tree and relating searching schemes [29–32]. As a result, one collision event in EDMD costs only about ten to twenty times more CPU time than a LMC trial move, even for large system sizes. EDMD drives the system quite efficiently through configuration space and clearly outperforms LMC. The simulations with this algorithm use an Intel Xeon E5-1660 CPU with a clock speed of 3.30GHz.

Event-chain Monte Carlo (ECMC) [6] replaces individual trial moves by a chain of collective moves that all translate particles in the same direction. At the beginning of each Monte Carlo move, a random starting disk and a move direction are selected. The starting disk is displaced in the chosen direction until it collides with another disk. This new disk is then displaced in the same direction until another collision occurs or until the lengths of all displacements add up to a total distance, an internal parameter of the algorithm which is typically chosen such that the chain consists of $\sim \sqrt{N}$ disks. With periodic boundary conditions, ECMC is free of rejections. Global balance and ergodicity are preserved by moving in two directions only, for example to the right and up. ECMC is faster than LMC and EDMD [6]. The simulations with this algorithm were performed on an Intel Xeon E5620 CPU with a clock speed of 2.40GHz.

For the large systems considered in this study, the ratio between the large absolute particle coordinates and the potentially small inter-particle distances becomes comparable to the accuracy of single floating point precision, so that round-off errors become critical. Different strategies allow us to cope with this problem. MPMC performs all computations in single-precision because today's GPUs run significantly slower in double-precision. We mitigate floating-point round-off errors by placing each particle in a coordinate system local to its cell. In this way, differences of relative positions are less affected by floating point precision than absolute positions. This strategy was also applied in [7]. EDMD calculations are performed in double-precision to fully resolve multiple coincident collisions and to span the entire time domain from individual collision times to total simulation time. The ECMC algorithm is implemented for this work in double-precision. We use this implementation to derive high-precision numbers at the density $\eta = 0.698$. Data points for ECMC at other densities are taken from Ref. [7], which employs single-precision. The comparison of single-precision and double-precision calculations at $\eta = 0.698$ indicates that the two versions of ECMC yield the same result for the pressure.

C. Pressure calculation

The complete statistical behavior of hard disks is contained in the equation of state (pressure vs. volume or density), which requires the precise evaluation of the internal pressure of the system. The equation of state allows computing the interfacial free energy and tracking the changes in the geometry of coexisting phase regions in a finite system (see [7, 21–23]).

In the NVT ensemble, the pressure is a dependent ob-

servable. In Monte Carlo, it has to be computed from static configurations while, in EDMD, it may in addition be derived from the collision rate. The disparity of our approaches to calculate pressure constitutes one more check for the implementations of our algorithms.

1. *Pressure from static configurations*

In systems of isotropic particles with pairwise interactions, the pressure can be computed from static configurations ("snapshots") through the pair-correlation function $g(r)$ [1]. The function $g(r)$ is defined as the distribution of particle pairs at distance $r = |\mathbf{x}_i - \mathbf{x}_j|$, normalized such that $g(r \to \infty) = 1$. In practice, particle distances are binned into a histogram with bin size δr. If n out of p pair distances are found to lie in the interval $[r - \delta r/2, r + \delta r/2]$, then we have

$$g(r) = \frac{n/p}{2\pi r \delta r / V}. \tag{2}$$

The pressure $P = -(\partial F/\partial V)_{T,N}$ is calculated from the free energy $F = -\beta^{-1} \ln Z$ and the partition function

$$\begin{aligned} Z &= \frac{1}{N!} \int_0^L \dots \int_0^L dx_1 .... dx_{2N} \theta(x_1 \dots x_{2N}) \\ &= \frac{V^N}{N!} \int_0^1 \dots \int_0^1 d\alpha_1 \dots d\alpha_{2N} \theta(\alpha_1 \dots \alpha_{2N}), \end{aligned} \tag{3}$$

where $\alpha_j = x_j/L$ are the particle coordinates relative to the simulation box. The Boltzmann weight θ is the characteristic function for overlap, *i.e.* zero if the configuration contains overlaps and one otherwise. A change of volume leaves the α unchanged, but rescales the positions and the pair distances. $\theta(\alpha_1 \dots \alpha_{2N})$ is only affected if one of the pair distances is at contact, hence

$$\begin{aligned} \beta P &= \frac{N}{V} + \frac{\sigma}{V} \left\langle \frac{\partial \theta}{\partial r} \right\rangle \Big|_{r=2\sigma^+} \\ &= \frac{N}{V} (1 + 2\eta\, g(2\sigma^+)). \end{aligned} \tag{4}$$

To access the contact value of $g(r)$, we fit the histogram of pair distances obtained from LMC by a polynomial as shown in Fig. 1 and then extrapolate the fit to $r = 2\sigma$ from the right. We choose the bin size as $\delta r = 10^{-3}\sigma$. The histogram is limited to $r \in [2\sigma, 2.1\sigma]$, and the fit is performed with a fourth-order polynomial. These parameters are sufficient to obtain a relative systematic error of less than 10^{-5}. In the single-precision version of the algorithm, $g(r)$ shows correlated fluctuations which lead to systematic errors in the value of $g(r)$ for any single bin (see Fig. 1(b,c)). These errors are only due to floating point round-off of the pair-correlation function (the sampled configurations are essentially the same). However, they are periodic with zero mean and do not affect the fit significantly. We verified that single-precision rounding induces a relative systematic error smaller than 10^{-5} on the estimated value of $g(2\sigma^+)$.

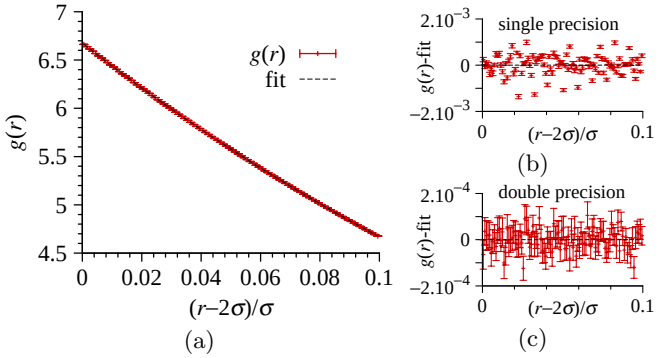

FIG. 1: (a) Pair-correlation function $g(r)$ close to contact for $N = 512^2$ at density $\eta = 0.698$ using LMC. Error bars are computed through 64 independent simulations. $g(r)$ is fitted with a fourth-order polynomial. Difference between $g(r)$ and the polynomial fit with the single-precision data (b) and double-precision data (c) for the histogram.

2. *Dynamic pressure computation*

In molecular dynamics, static configurations can be analyzed as before, but the pressure is computed directly and more efficiently from the collision rate via the virial theorem [33–35]. This avoids binning and extrapolations. The non-dimensional virial pressure in two dimensions is given by

$$\beta P = \frac{N}{V} \left[1 - \frac{\beta m}{2 t_{\text{tot}}} \frac{1}{N} \sum_{\text{collisions}} b_{ij} \right] \tag{5}$$

where t_{tot} is the total simulation time. The collision force $b_{ij} = \mathbf{r}_{ij} \cdot \mathbf{v}_{ij}$ is defined between the relative positions and relative velocities of the collision partners. In equilibrium, the average virial for hard disks equals [36]

$$\langle b_{ij} \rangle = -2\sigma \sqrt{\frac{\pi}{\beta m}}. \tag{6}$$

Therefore, the pressure is simply given by the collision rate $\Lambda = 1/t_0$, the reciprocal of the mean free time t_0, as

$$\beta P = \frac{N}{V} \left[1 + \frac{\sigma \sqrt{\pi \beta m}}{2} \Lambda \right]. \tag{7}$$

To test the pressure calculations, we compute the pressure with all algorithms at one representative state point. With each algorithm, we perform between 8 and 100 independent runs to compute the statistical standard error. Results obtained with the four algorithms agree within numerical accuracy to $\leq 10^{-4}$, which is sufficient for our purposes (see Table I).

III. PERFORMANCE COMPARISON

One of the slowest processes during the time evolution of the hard-disk system at high density is the fluctuation

Algorithm	#runs	#disp/run	$\beta P(2\sigma)^2$	std. error
LMC	64	6×10^{11}	9.17046	1.5×10^{-4}
EDMD	100	10^{10}	9.17076	1.8×10^{-4}
ECMC	32	5×10^{11}	9.17062	8.7×10^{-5}
MPMC	8	6×10^{13}	9.17078	4.5×10^{-5}

TABLE I: Test of the pressure computations for $N = 256^2$ at $\eta = 0.698$ Results of all four algorithms agree within their numerical accuracies.

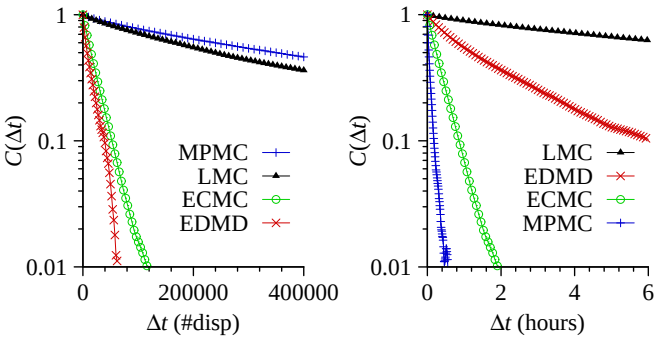

FIG. 2: Autocorrelation function of the global orientation order parameter $\Psi_6(t)$ for $N = 512^2$, $\eta = 0.698$ obtained with LMC, EDMD, ECMC, and MPMC.(a) Time is measured in number of attempted displacements (or collisions) per disk. (b) Time is measured in CPU or GPU hours.

of the global orientation order parameter

$$\Psi_6 = \frac{1}{N} \sum_j \psi_j,$$

which is the spatial average of the local order-parameter field

$$\psi_j = \frac{1}{6} \sum_{k=1}^{6} \exp(i\, 6\phi_{j,k}). \tag{8}$$

The sum is over the six closest neighbors k of disk j, and $\phi_{j,k}$ is the angle between the shortest periodic vector equivalent to $\mathbf{x}_k - \mathbf{x}_j$ and a chosen fixed reference vector. This approach is simpler than using the Voronoi construction [7], without affecting the autocorrelation functions. To determine the efficiency of our algorithms, we track the autocorrelation function of Ψ_6 [6],

$$C(\Delta t) = \frac{\langle \Psi_6(t) \Psi_6^*(t + \Delta t) \rangle_t}{\langle |\Psi_6|^2 \rangle}. \tag{9}$$

The $\Psi_6 \to \Psi_6 + \pi$ symmetry in the square box imposes that $C(\Delta t)$ decays to zero for infinite times. In the asymptotic limit, the decay is exponential, $C(\Delta t) \propto \exp(-\Delta t/\tau)$, and we obtain the correlation time τ from a fit of the pure exponential part (see Fig. 2).

We compare speeds for $N = 512^2$ at $\eta = 0.698$, that is, in the dense liquid close to the liquid-hexatic coexistence.

Algorithm	τ/#disp	#disp/hour	$\tau_{\rm LMC}/\tau$	Speed-up
LMC	7×10^5	6.5×10^9	1	1
EDMD	1.8×10^4	1.7×10^9	39	10
ECMC	2.5×10^4	1.6×10^{10}	28	70
MPMC	8×10^5	2.3×10^{12}	0.9	320

TABLE II: Speed comparison of the four hard-disk algorithms for $N = 512^2$, $\eta = 0.698$. The correlation time τ is measured in number of displacements (disp) per disk. #disp/hour represents the number of displacements (or collisions) per hour achieved in our implementations. The two rightmost columns show the speed-up of the algorithms in number of displaced disks, and in terms of CPU or GPU time in comparison to LMC.

Although still a liquid, the correlation length of the local orientational order parameter ψ_j at this density is $\sim 50\sigma$. Such a large correlation *length* induces a long correlation *time*, and equilibration requires $> 10^6$ trial moves per disk for LMC. For the test, each algorithm is set to its optimal internal parameters. Total simulation run times are on the order of $10^3\tau$ to $10^4\tau$.

Fig. 2 illustrates that the autocorrelation functions decay roughly as pure exponentials. The time unit in Fig. 2(a) corresponds to the number of attempted displacements per disk (number of collisions in the case of EDMD and ECMC). As expected, MPMC decays slightly more slowly than LMC because trial moves across cell boundaries are rejected. ECMC and EDMD are significantly faster than LMC, confirming that these two methods sample configuration space more efficiently, but slower than MPMC. The time unit in Fig. 2(b) corresponds to the real simulation time (CPU or GPU time).

Correlation times, number of attempted displacements per hour, and accelerations with respect to LMC are summarized in Table II. EDMD and ECMC sample configuration space more efficiently by a factor of 39 times and 28 times, respectively, while MPMC samples configuration space slightly less efficiently by a factor of 0.9. Evidently, the efficiency of the simple LMC algorithm is improved significantly with speed-ups of 10, 70, and 320 for EDMD, ECMC, and MPMC, respectively. Although speeds in Table II correspond to somewhat different hardware, as indicated in the methods section, the numbers give a clear idea of practical improvements that can be obtained with respect to LMC.

IV. RESULTS

A. Equation of state at high density

In their seminal work, Alder and Wainwright observed a loop in the equation of state of hard disks [3]. As explained by Mayer and Wood [21] (see also [22, 23]), this loop is a result of finite simulation sizes and therefore differs conceptually from a classic van der Waals loop, which

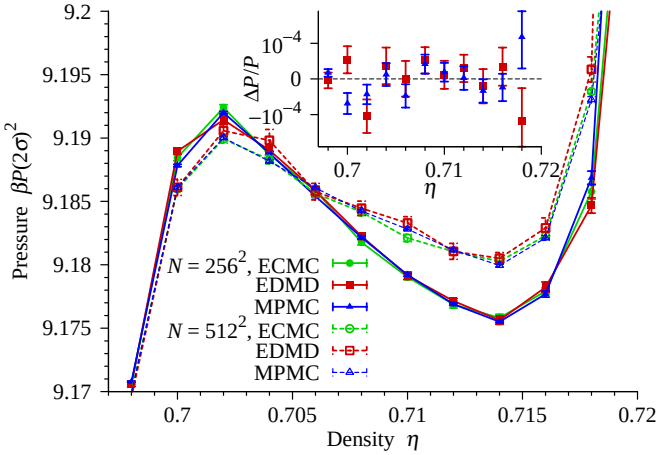

FIG. 3: Equation of state from ECMC, EDMD, and MPMC for $N = 256^2$ and $N = 512^2$. Error bars are mostly smaller than the symbols. Results agree within standard deviation. The inset shows the relative pressure difference $\Delta P/P$ of EDMD and MPMC with respect to ECMC for $N = 256^2$.

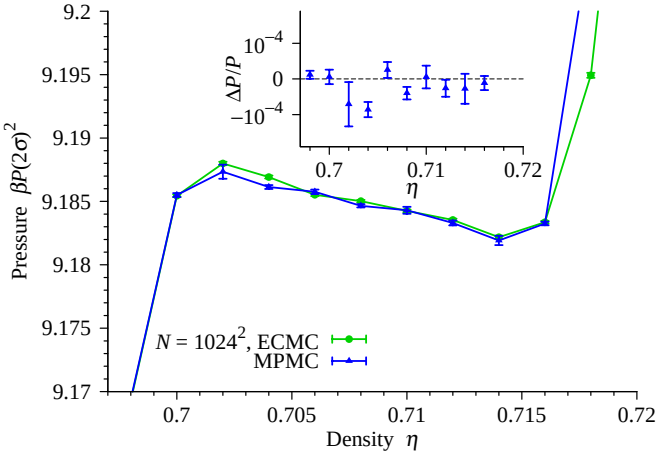

FIG. 4: Equation of state from ECMC and MPMC for $N = 1024^2$. Error bars for ECMC are smaller than the symbols. Results agree within standard deviation. The inset shows the relative pressure difference $\Delta P/P$ of MPMC with respect to ECMC.

is derived in the thermodynamic limit. The branches of the Mayer-Wood loop are thermodynamically stable, but vanish in the limit of infinite size.

It is known that the presence of a Mayer-Wood loop in the equation of state is observed in systems showing a first-order transition as well as systems showing a continuous transition [37]. However, the behavior of these loops with increasing system size is different. For a first-order transition, the loop is present in the coexistence region and is caused by the interface free energy ΔF. At a given density, the interface free energy per disk, $\Delta f = \Delta F/N$, can be computed by integrating the equation of state [7]. In two dimensions, it scales as $\Delta f \propto N^{-1/2}$. In contrast, for a continuous transition, Δf decays faster, normally such that ΔF is constant, that is $\Delta f \propto N^{-1}$, and the equation of state becomes monotonic for large enough systems. The scaling of Δf with system size, together with a fixed finite separation of the peaks for large system sizes, is a reliable indicator of the first-order character of a phase transition [38].

Fig. 3 shows the equation of state for $N = 256^2$ and $N = 512^2$, obtained with ECMC, EDMD, and MDMC. Error bars (standard errors) are computed through independent simulations. The inset shows the relative pressure difference $\Delta P/P$ of EDMD and MDMC with ECMC. Error bars correspond again to the standard error on $\Delta P/P$. We observe that the three independent simulations agree. In a similar way, Fig. 4 compares results from ECMC and MPMC for $N = 1024^2$. For this system size and the currently available computer hardware, equilibration with EDMD takes too long to be practical. Again, all results agree within standard deviations. Note that while the Mayer-Wood loop shrinks with system size, the position of the local extrema stay fixed close to $\eta = 0.702$ and $\eta = 0.714$.

B. Orientational order using simulation snapshots

In [7], the orientational order parameter field was graphically represented for individual configurations at densities where coexistence occurs to show the separation of the liquid and the hexatic phase. The characteristic geometry of the region of the minority phase with increasing density, from a circular bubble into a parallel stripe and again into a circular bubble, was directly observed. The spatial correspondence between variations in local density and orientational order provided important evidence for the nature of the transition.

Ref. [7] used the projection of the local orientational order ψ_k on the global orientational order Ψ_6 and a linear color code. This projection is by no means a unique measure for the orientational order parameter field. Instead, in Fig. 5, we use a circular color code on data obtained by long MPMC simulations with $N = 1024^2$. At $\eta = 0.700$, the system is completely liquid and the color fluctuates on the scale of the correlation length. At $\eta = 0.704$, the representations once more confirm the presence of a circular bubble of hexatic phase, visible as a large region of constant color (purple), whereas at $\eta = 0.708$ a stripe minimizes the interfacial free energy. The hexatic phase is now visible in blue, while the liquid is characterized by fluctuations of the direction of Ψ_6. The constant color in the region of the hexatic phase confirms the presence of the same orientational order across the system.

C. Positional correlation functions

To identify the nature of the high-density phase, we analyze the positional order in the system. The goal is to distinguish the hexatic phase, which has short-range positional order (exponential decay) and quasi-

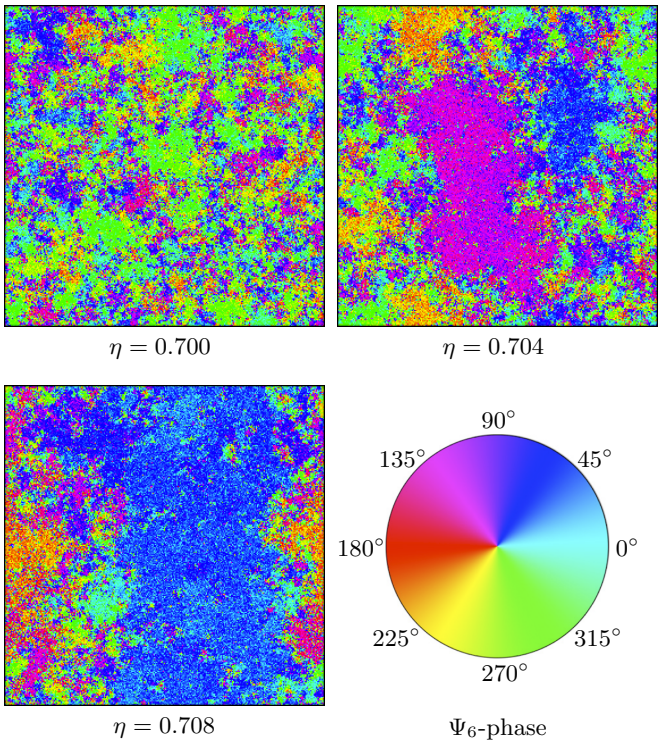

FIG. 5: Snapshots of configurations obtained with the MPMC algorithm for $N = 1024^2$. With increasing density, pure liquid ($\eta = 0.700$), a bubble of hexatic phase ($\eta = 0.704$), and a stripe regime of hexatic phase ($\eta = 0.708$) are visible. The Ψ_6-phase is color-coded according to the color wheel. The interface between the liquid and the hexatic phase is extremely rough.

long-range orientational order (algebraic decay), from the two-dimensional solid, which has quasi-long range positional order and long-range orientational order (no complete decay). In [7], the positional order was analyzed primarily using the two-dimensional pair-correlation function in direct space. We now complement that work by an analysis of the positional correlation function in reciprocal space [40],

$$C_{\mathbf{q}}(r) = \langle \exp(i\mathbf{q} \cdot (\mathbf{x}_n - \mathbf{x}_m)) \rangle \,. \tag{10}$$

Here, the average is done over neighboring pairs that satisfy $|\mathbf{x}_n - \mathbf{x}_m| \in [r - \sigma, r + \sigma]$. With this classic method, the wave vector $\mathbf{q}$ must be chosen carefully to correspond to a diffraction peak. In some previous works [13, 39], the assumption was made that $\mathbf{q}$ would correspond to the reciprocal vector of a perfect triangular lattice of edge length a_0, namely $|\mathbf{q}| = 2\pi/(a_0\sqrt{3}/2)$. This assumption is not correct because the solid phase has a finite density of vacancies and other defects in equilibrium, which increases the effective lattice constant [7].

In the present work, $\mathbf{q}$ corresponds to the maximum value of the first diffraction peak of the structure factor

$$S(\mathbf{q}) = \frac{1}{N} \sum_{n,m} \exp(i\mathbf{q} \cdot (\mathbf{x}_n - \mathbf{x}_m)). \tag{11}$$

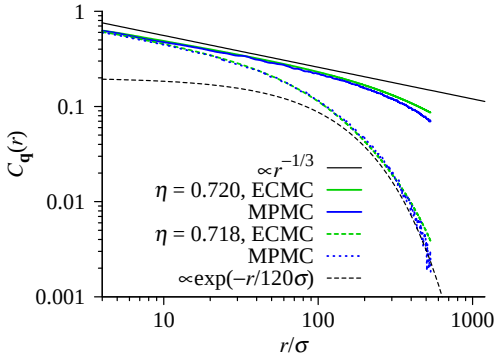

FIG. 6: Positional correlation functions $C_{\mathbf{q}}(r)$ for $N = 512^2$. Results obtained with ECMC and MPMC agree. At density $\eta = 0.718$, the decay is exponential. At density $\eta = 0.720$, the decay approaches a power law $\propto r^{-1/3}$. See [7] for data at $N = 1024^2$.

As the system can perform global rotations during the simulations, $\mathbf{q}$ rotates from one configurations to the other. To compute a precise average value of $S(\mathbf{q})$, we individually rotate configurations so that Ψ_6 is aligned in the same direction for all of them.

Fig. 6 shows $C_{\mathbf{q}}(r)$ for $N = 512^2$ at $\eta = 0.718$ and $\eta = 0.720$. The results of ECMC and MPMC are again in good agreement. We observe that $C_{\mathbf{q}}(r)$ decays exponentially at $\eta = 0.718$. Therefore, $\eta = 0.718$ cannot be in the solid phase. At $\eta = 0.720$, the positional order increases drastically. $C_{\mathbf{q}}(r)$ decays almost as a power law, $r^{-1/3}$, which is the stability limit for the solid phase. Since the coexistence phase ends at $\eta \simeq 0.716$, the region $\eta \in [0.716, 0.720]$ is thus hexatic and the first-order transition observed in Fig. 3 connects a liquid and a hexatic phase.

V. CONCLUSION

We computed the thermodynamic behavior of the hard-disk system close to the melting transition using independent implementations of three different simulation algorithms to sample configuration space and two distinct approaches for the pressure computation. The equation of state data, including error bars, of Ref. [7] are confirmed within numerical accuracy both qualitatively and quantitatively. Typical relative errors are $\lesssim 10^{-4}$, more than one order of magnitude smaller than finite-size effects for systems with up to $N = 1024^2$ particles. Such finite-size effects are manifested in the form of a Mayer-Wood loop in the equation of state. Our analysis of orientational and positional correlation functions confirms the presence of a first-order phase transition from liquid order to hexatic order.

Acknowledgments

J.A.A., M.E. and S.C.G acknowledge support by the Assistant Secretary of Defense for Research and Engineering, U.S. Department of Defense, N00244-09-1-0062. The massively parallel MC simulations were performed on a GPU cluster hosted by the University of Michigan's Center for Advanced Computing. M.I. is grateful for financial support from the CNRS-JSPS Researcher Exchange Program for staying at ENS-Paris and Grant-in-Aid for Scientific Research from the Ministry of Education, Culture, Sports, Science and Technology No. 23740293. The event-driven molecular dynamics simulations were partially performed using the facilities of the Supercomputer Center, ISSP, Univ. of Tokyo, and RCCS, Okazaki, Japan. W.K. acknowledges the hospitality of the Aspen Center for Physics, which is supported by the National Science Foundation Grant No. PHY-1066293. W.K. acknowledges helpful correspondence from D. Fiocco.

[1] N. Metropolis, A. W. Rosenbluth, M. N. Rosenbluth, A. H. Teller, E. Teller, *J. Chem. Phys.* **21** 1087 (1953).
[2] B. J. Alder, T. E. Wainwright, *J. Chem. Phys.* **27**, 1208 (1957).
[3] B. J. Alder, T. E. Wainwright, *Phys. Rev.* **127**, 359 (1962).
[4] K. J. Strandburg, *Rev. Mod. Phys.* **60**, 161 (1988).
[5] J. G. Dash, *Rev. Mod. Phys.* **71**, 1737 (1999).
[6] E. P. Bernard, W. Krauth, D. B. Wilson, *Phys. Rev. E* **80**, 056704 (2009).
[7] E. P. Bernard, W. Krauth, *Phys. Rev. Lett.* **107**, 155704 (2011).
[8] J. M. Kosterlitz, D. J. Thouless, *J. Phys. C* **5**, L124 (1972).
[9] B. I. Halperin, D. R. Nelson, *Phys. Rev. Lett.* **41**, 121 (1978).
[10] D. R. Nelson, B. I. Halperin, *Phys. Rev. B* **19**, 2457 (1979).
[11] A. P. Young, *Phys. Rev. B* **19**, 1855 (1979).
[12] A. Jaster, *Phys. Rev. E* **59**, 2594 (1999).
[13] C. H. Mak, *Phys. Rev. E* **73**, 065104 (2006).
[14] D. S. Fisher, B. I. Halperin, R. Morf, *Phys. Rev. B* **20**, 4692 (1979).
[15] S. T. Chui, *Phys. Rev. B* **28**, 178 (1983).
[16] H. Kleinert, *Phys. Lett. A* **95**, 381 (1983).
[17] T. V. Ramakrishnan, *Phys. Rev. Lett.* **48**, 541 (1982).
[18] H. Weber, D. Marx, K. Binder, *Phys. Rev. B* **51**, 14636 (1995).
[19] J. A. Zollweg, G. V. Chester, *Phys. Rev. B* **46**, 11186 (1992).
[20] J. Lee, K. J. Strandburg, *Phys. Rev. B* **46**, 11190 (1992).
[21] J. E. Mayer, W. W. Wood, *J. Chem. Phys.* **42**, 4268 (1965).
[22] H. Furukawa, K. Binder, *Phys. Rev. A* **26**, 556 (1982).
[23] M. Schrader, P. Virnau, K. Binder, *Phys. Rev. E* **79**, 061104 (2009).
[24] J. A. Anderson, E. Jankowski, T. L. Grubb, M. Engel, S. C. Glotzer *submitted*.
[25] M. Isobe, *Int. J. Mod. Phys. C* **10**, 1281 (1999).
[26] W. Krauth, *Statistical Mechanics: Algorithms and Computations*, Oxford University Press (2006).
[27] A. Uhlherr, S. J. Leak, N. E. Adam, P. E. Nyberg, M. Doxastakis, V. G. Mavrantzas, D. N. Theodorou, *Comp. Phys. Commun.* **144**, 1 (2002).
[28] G. Pawley, K. Bowler, R. Kenway, D. Wallace, *Comp. Phys. Commun.* **37**, 251 (1985).
[29] D. C. Rapaport, *J. Comp. Phys.* **34**, 184 (1980).
[30] B. D. Lubachevsky, *J. Comp. Phys.* **94**, 255 (1991).
[31] M. Marin, D. Risso, P. Cordero, *J. Comp. Phys.* **109**, 306 (1993).
[32] M. Marin, P. Cordero, *Comp. Phys. Commun.* **92**, 214 (1995).
[33] J. J. Erpenbeck, W. W. Wood, in *Modern Theoretical Chemistry Vol.6, Statistical Mechanics Part B*, edited by B. J. Berne (Plenum, New York, 1977).
[34] B. J. Alder, T. E. Wainwright, *J. Chem. Phys.* **33**, 1439 (1960).
[35] W. G Hoover, B. J. Alder, *J. Chem. Phys.* **46**, 686 (1967).
[36] A. C. J. Ladd, W. E. Alley, B. J. Alder, *J. Stat. Phys.* **48**, 1147 (1987).
[37] J. J. Alonso, J. F. Fernández, *Phys. Rev. E* **59**, 2659 (1999).
[38] J. Lee, J. M. Kosterlitz, *Phys. Rev. B* **43**, 3265 (1991).
[39] K. Bagchi, H. C. Andersen, W. Swope, *Phys. Rev. Lett.* **76**, 255 (1996).
[40] For a detailed discussion and analysis of correlation functions see also the supplemental material of [7].